Rate Effects on the Uplift Capacity of Pipelines Embedded in Clay: Finite Element Modelling

Brian B. Sheil[1]*, Byron W. Byrne[1] and Christopher M. Martin[1]

[1]Department of Engineering Science, University of Oxford, Parks Road, Oxford OX1 3PJ, UK

*Email: brian.sheil@eng.ox.ac.uk. Tel.: +44 (0)1 865 273170

ABSTRACT

This paper describes a finite element study of the uplift behaviour of a plane strain pipe segment embedded in modified Cam clay soil. The primary aim of this study is to explore the role of rate effects on pipe uplift capacity and the transition between drained and undrained behaviour using coupled-consolidation analyses. The velocities considered in the modelling cover six orders of magnitude allowing a rigorous assessment of the effect of loading rate. The effects of pipe embedment depth, soil strength profile and pipe-soil interface roughness are also investigated. The results indicate that the range of uplift velocities for which the soil response can be considered 'partially drained', as determined from the peak uplift resistances, is significant and exceeds bounds established for full flow penetrometers previously reported in the literature. The data also suggests that excess pore pressures determined locally at the pipe-soil interface may not be a reliable means of determining whether the overall response is 'drained' or 'undrained'. To address some limitations associated with design guidelines currently used by industry, a new approach for the prediction of pipe uplift capacity as a function of loading rate is proposed and applied to a hypothetical design scenario.

Keywords: uplift; finite element; rate effects; upheaval buckling; buried pipeline; clay

INTRODUCTION

Pipelines used for the offshore oil and gas industry in shallow water depths are frequently buried below ground to provide thermal insulation, pipeline stability, and to protect them from mechanical damage from above-ground activities. When transporting hot pressurised fluids, pipelines can experience unburial to relieve thermal stresses that build up in the pipe walls, commonly through upheaval buckling. This is where sections of pipe move upward through the soil cover, possibly to the extent where they become exposed at the soil surface. One of the main uncertainties in the design calculation for this scenario is the soil resistance to the upward movement. Given the extensive system of pipelines required in the production of offshore oil and gas, there is significant motivation to optimise burial depths towards more economical design.

While drained uplift is often the limiting design case for offshore buried pipelines, there is a general lack of consensus regarding pipe uplift rates that constitute ‘drained’ and ‘undrained’ behaviour in clay. Bransby et al. (2002) reported results from a series of centrifuge tests to explore the uplift behaviour of pipes buried in recently liquefied clay subjected to both ‘short-term’ and ‘long-term’ loadings. Those authors observed that the short-term condition was critical for pipes embedded in unconsolidated clay. These findings are also supported by Cheuk et al. (2007) from centrifuge tests exploring the influence of jetting (and subsequent consolidation) on the vertical pressure acting on pipe sections buried in ‘lumpy’ clay. The results showed that early commissioning of buried pipelines in unconsolidated clay can reduce the vertical soil restraint by up to 56%. Those authors also noted that the suction force that develops beneath the pipe is a major contributor of the overall uplift resistance. Thusyanthan et al. (2008) and Wang et al. (2009) described centrifuge tests of pipe uplift in homogenous and ‘blocky’ clay respectively where the soil was allowed to consolidate after pipe installation. In this case, both studies confirmed that ‘slow’ uplift rates yielded lower pipe uplift resistance compared to ‘fast’ uplift rates. Martin and White (2012) explored the ultimate bearing capacity of a rigid plane strain pipe segment embedded in undrained clay using finite

element (FE) limit analysis. The study highlighted the importance of the tension (suction) boundary condition at the pipe-soil interface during undrained uplift.

Although the design rules set out in DNV (2017) provide some guidance as to the appropriate calculations to use for the assessment of uplift capacity, only the two extreme rates of uplift (drained and undrained) are considered. To address this limitation, this paper presents results from a series of constant-rate pipe uplift FE analyses with uplift rates covering six orders of magnitude. A plane strain pipe section is considered 'wished in place' in modified Cam clay soil. The primary aim of this study is to explore the role of rate effects on pipe uplift capacity and the transition between drained and undrained behaviour using coupled-consolidation calculations. The guidance provided by the DNV (2017) design codes is appraised through comparisons to the FE results. Results from the FE modelling are subsequently used to inform the development of a simplified closed-form expression, amenable for use in routine design, for the prediction of pipe uplift capacity as a function of uplift velocity.

DNV-RP-F114 (2017) GUIDELINES

The calculation for the drained uplift capacity outlined in DNV (2017) uses a vertical slip model (VSM). This method is predicated on the assumption that soil failure consists of an upward heave of a sliding block bounded by shear planes (Trautmann et al. 1985, Schaminee et al. 1990). The uplift resistance, V, can be defined as follows (DNV 2017):

$$V = \gamma' \cdot H \cdot D + \gamma' \cdot D^2 \cdot \left(\frac{1}{2} - \frac{\pi}{8}\right) + K \cdot \tan\phi' \cdot \gamma' \cdot \left(H + \frac{D}{2}\right)^2 \quad (1)$$

where K is the 'operational' coefficient of lateral earth pressure, γ' is the effective unit weight of the soil backfill, ϕ' is the soil friction angle, H is the cover height measured from the pipe crown and D is the pipe diameter. For a 'lumpy clay', values of K back-calculated from full-scale laboratory test results correspond to the in-situ 'at rest' value, K_0 (0.29 – 0.67 with a mean of 0.51; Chen et al. 2016). An obvious limitation to the DNV (2017) approach is the

difficulty in predicting the development of *K* during uplift due to the changing geometry and disturbance of the soil as the pipe is displaced vertically.

The undrained resistance is determined by one of two modes that apply: (a) 'global' soil failure with a mechanism that extends to the soil surface or (b) 'local' soil failure with a flow-round mechanism that is local to the pipe, independent of depth. It is likely that the global mechanism applies for shallowly embedded pipes, with the local mechanism becoming critical (i.e. giving a lower uplift resistance) at deeper embedment. The 'global' soil failure mode uses an undrained form of the VSM:

$$V = \gamma' \cdot H \cdot D + \gamma' \cdot D^2 \cdot \left(\frac{1}{2} - \frac{\pi}{8}\right) + 2 \cdot \overline{s_u} \cdot \left(H + \frac{D}{2}\right) \quad (2)$$

where $\overline{s_u}$ is the average undrained shear strength along failure planes extending from the centre of the pipe to the soil surface, reflecting the strength of the trenched material. This equation neglects any allowance for the suction that would be likely to develop beneath the pipe. The 'local' failure resistance is given by:

$$V = N_c \cdot \overline{s_u} \cdot D - \gamma' \cdot A_p \quad (3)$$

where A_p is the cross-sectional area of the pipe and N_c is the undrained bearing capacity factor. The recommended range for N_c is 9 – 12 which approximates the plasticity solutions documented by Randolph and Houlsby (1984).

FINITE ELEMENT MODEL

Geometry and material parameters

In this study, a total of 180 displacement FE analyses were undertaken to explore the influence of rate effects on the uplift resistance of a buried pipeline in clay using the FE software program Plaxis 2D Version 2016.1. Coupled-consolidation analyses were completed assuming plane strain conditions. Figure 1 defines the relevant variables for this study along with the dimensions of the computational domain. The pipe has a diameter *D* of

1 m (fixed) and a cover height, H, varying between one and four pipe diameters. The uplift resistance is V, the upward displacement and velocity of the pipe are denoted w and v respectively and their respective normalisations are listed in Table 1. The pipe is considered buried in a trench filled with soil of undrained shear strength s_u (varying with depth), effective unit weight γ', and coefficient of consolidation c_v. For consistency across various strength profiles, the pipe uplift resistance under (assumed) undrained conditions is always normalised using the initial undrained strength of the soil at the level of the pipe springline, denoted s_{u0}.

Table 1 Parameter normalisation adopted in this study

Normalised variable	Non-dimensional form
Embedment depth, $\hat{H}$	H/D
Uplift resistance, $\hat{V}$	$V/s_{u0}D$
Uplift displacement, $\hat{w}$	w/D
Uplift velocity, $\hat{v}$	vD/c_v
Excess pore pressure, $\Delta\hat{u}$	$\Delta u/s_{u0}$
Effective soil stress, $\hat{\sigma}'$	σ'/s_{u0}

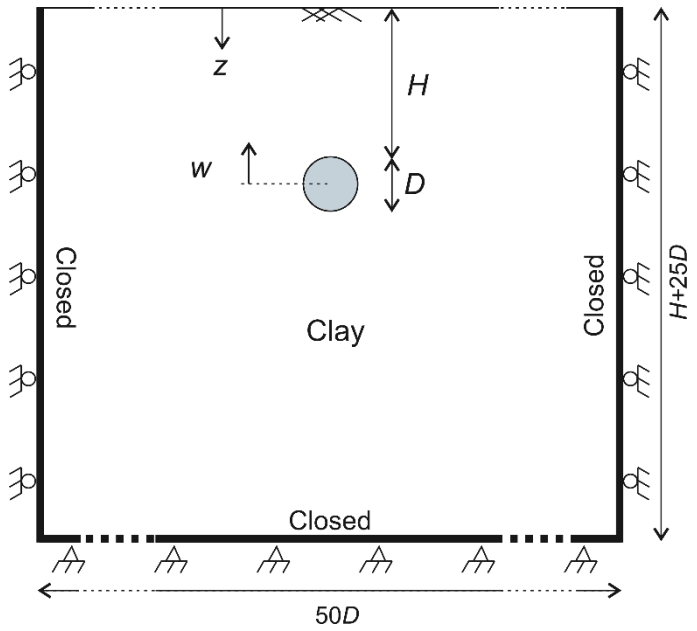

Fig. 1 Problem definition and geometry

The pipe was modelled as a rigid body. Separation between the pipe and soil was allowed (but not imposed) when σ'_v was less than zero using interface elements. In the present analyses, the pipe is always fully embedded so the formation of a gap between pipe and soil can only occur as a result of seepage of pore water from the surrounding soil. The pipe-soil interface was modelled as an elastic−plastic Tresca material with an undrained shear strength of $s_{u0,int} = \alpha \cdot s_{u0}$, shear stiffness of 1 MPa and normal stiffness of 100 MPa where α is the soil-structure interface roughness. High stiffness values were assigned to the interface to approximate rigid-plastic interface behaviour whilst also avoiding numerical ill-conditioning. The modified Cam clay constitutive model was adopted to simulate the behaviour of the soil backfill. Four different soil profiles are considered in the modelling and the input parameters for each are presented in Table 2. The variation of undrained shear strength with depth (obtained from the FE output) for each soil profile is shown in Fig. 2.

Table 2 Input parameters for the four soil profiles adopted in the FE modelling

Parameter	Value			
	Soil profile 1	Soil profile 2	Soil profile 3	Soil profile 4
Slope of critical state line, M	0.98 (ϕ' = 25°)	1.2 (ϕ' = 30°)	1.42 (ϕ' = 35°)	1.2 (ϕ' = 30°)
Slope of normal compression line, λ	0.1	0.1	0.1	0.1
Slope of unloading-reloading line, κ	0.02	0.02	0.02	0.02
Effective Poisson's ratio, ν'_{ur}	0.3	0.3	0.3	0.3
Effective unit weight, γ' (kN/m^3)	6	6	6	6
Permeability, k (m/day)	1×10^{-5}	1×10^{-5}	1×10^{-5}	1×10^{-5}
Coefficient of lateral earth pressure at rest, K_0 (= 1 – sinϕ')	0.58	0.5	0.43	0.5
Overconsolidation ratio, OCR	1	1	1	Variable[a]

[a] *A variable OCR profile (with depth) was created by imposing a pre-overburden pressure (POP) = 50 kPa where POP is defined as the difference between the preconsolidation pressure and the current vertical effective stress.*

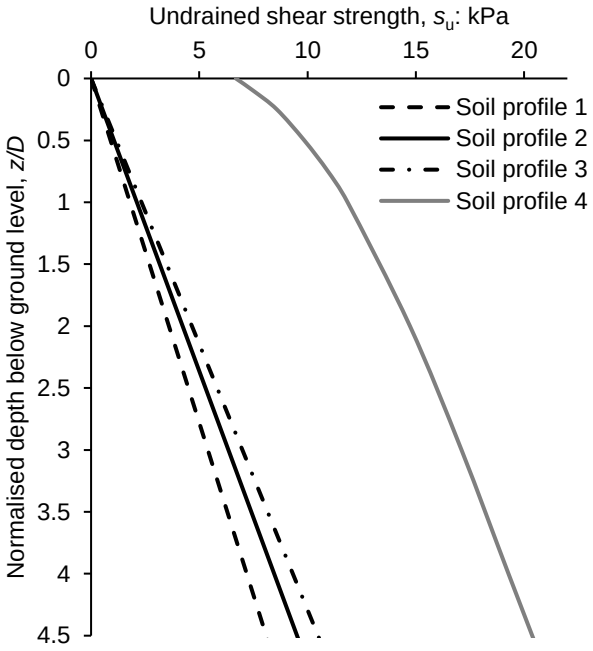

Fig. 2 Variation of undrained shear strength with normalised depth for the four soil strength profiles considered in the numerical modelling. Corresponding soil parameters are listed in Table 2.

When considering the likely degree of drainage for a penetrometer or buried pipe in fine-grained soil, the velocity is typically normalised as vD/c_v. This is derived by adopting a representative consolidation time for a drainage path of length D (i.e. D^2/c_v), normalised by a representative time for the loading event, equivalent to a movement through one diameter (i.e. $t = D/v$). Drained or undrained behaviour can be achieved depending on the value of this normalised quantity, with bounds established for full flow penetrometers e.g. Randolph and House (2001). The parameter c_v was determined from an input of the coefficient of permeability, k. For soil profiles 1 – 3 (normally consolidated soil) this was determined as follows (Wood 1990):

$$c_v = \frac{k(1+e_0)\sigma'_v}{\lambda\gamma_w} \quad (4)$$

where e_0 is the initial void ratio which is taken as 1.5, σ'_v is the vertical effective stress taken at the pipe springline, λ is the slope of the normal consolidation line and γ_w is the unit weight

of water. For profile 4 (overconsolidated soil), λ is replaced with the slope of the unload reload line, κ in equation (4).

The 'base case' pipe / soil parameters adopted for this study are listed in Table 3. In this paper, the terms 'smooth' and 'rough' are used to denote values of α of 0 and 1 respectively. A smooth interface is most representative of the pipe coatings typically adopted offshore, with any resulting bias on the safe side. Smooth pipes therefore represent the focus of this study. A limited number of analyses using a rough interface have also been included for comparison, however. A value of α = 1 was achieved numerically by adopting a high interface strength ($s_{u0,int}$ = 1 MPa) such that failure is promoted in the soil medium rather than at the pipe-soil interface.

Table 3 Pipe / soil parameters adopted for base case

Parameter	Value
Pipe diameter, D (m)	1.0
Normalised embedment depth, $\hat{H}$	2.5
Soil profile (Fig. 2, Table 2)	2
Interface roughness	0 (perfectly smooth)
Normalised uplift velocity, $\hat{v}$	Fully drained, 1×10^{-4}, 3×10^{-4}, 1×10^{-3}, 3×10^{-3}, 0.01, 0.03, 0.1, 0.3, 1, 3, 10, 30, 100, fully undrained

Finite element mesh

The soil was modelled using fourth-order, 15-node triangular elements while the pipe structure was modelled using 5-node beam elements. An exemplar finite element mesh is shown in Fig. 3. The same mesh density was maintained in the region immediately surrounding the pipe in all analyses. The lateral boundaries were restricted from movement normal to the respective surface whereas the bottom boundary was restrained from movement in both directions. The top drainage boundary was set as 'open' to allow dissipation of pore pressure, whereas all other drainage boundaries were 'closed'.

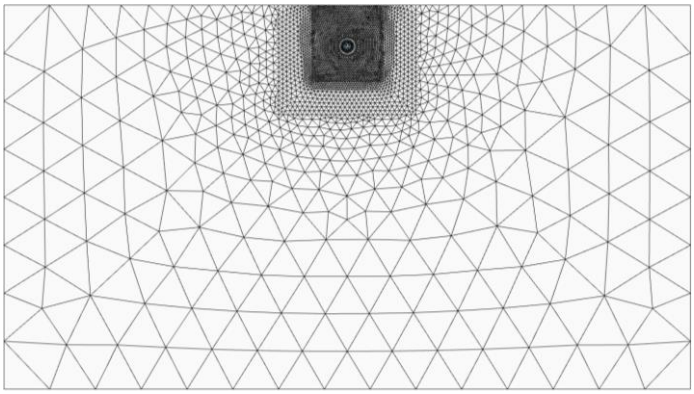

Fig. 3 Exemplar finite element mesh adopted for base case showing increased mesh density in zone immediately surrounding buried pipe; $\hat{H}$ = 2.5, ~9000 elements

Finite element calculation stages

The calculation stages adopted in the analyses are as follows:

1. Initialisation of soil stresses.
2. 'Wished in place' installation of a weightless, rigid pipe. The pipe was restrained from movement during this calculation phase.
3. Application of a constant upward pipe velocity during a coupled-consolidation phase. This was achieved by prescribing an upward displacement of 0.1D to the pipe over a specified time interval. The time interval was varied to achieve normalised uplift rates, $\hat{v}$, ranging between 1×10^{-4} and 1×10^{2} (see Table 3) where $\hat{v} = vD/c_v$. Rotation of the pipe was prevented during uplift.

Validation

To validate the numerical model and the adopted mesh density, predictions of pipe uplift capacity under undrained loading (no consolidation allowed) from Plaxis were compared with OxLim. OxLim is an in-house finite element limit analysis program developed by C.M. Martin. It uses the classical assumptions of limit analysis: all materials and interfaces are rigid–plastic and obey the associated flow (or normality) rule. In OxLim it is also possible to model rigid

bodies, and it is convenient to treat the plane-strain pipe segment in this way. The program computes both lower and upper bound collapse loads. Adaptive remeshing is used to ensure that these bounds bracket the exact collapse load very closely (typically to within 1% or better). An advantage of using OxLim is that the critical failure mechanism is automatically obtained for the geometry and undrained strength profile of each specific case, rather than requiring the assessment of multiple hypothetical failure mechanisms. The interested reader is referred to Makrodimopoulos and Martin (2006, 2007, 2008) and Martin (2011) for additional information. Predictions of the base case uplift capacity determined using Plaxis are compared with those computed using OxLim (assuming full-tension interface conditions) in Fig. 4 where very good agreement can be observed this giving confidence in the adopted modelling procedures.

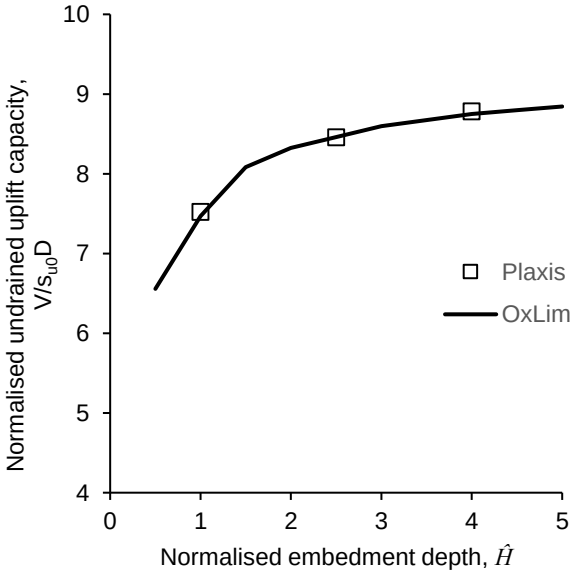

Fig. 4 Comparison between Plaxis and OxLim predictions of pipe uplift capacity during fully undrained loading; soil profile 2, α = 0, tension allowed

Comparison with DNV (2017)

Figure 5 compares FE predictions of the drained and undrained uplift capacity to those calculated using the DNV (2017) design rules for the base case. It can be seen that there is

good agreement between both sets of drained predictions provided an appropriate value of K (= 0.5; see Table 2) is adopted for use in equation (1). For the DNV (2017) 'undrained local' calculation, the minimum recommended value of N_c = 9, corresponding to α = 0, has been adopted. It can be seen that this calculation provides an upper-bound prediction of the FE results. This is to be expected as the recommended values of N_c in DNV (2017) correspond to a deep failure mechanism in uniform soil applied to laterally loaded piles (Randolph and Houlsby 1984). This underlines the importance of selecting case-specific values of N_c for use in equation (3) such as those reported in Martin and White (2012). By contrast, the undrained capacity is significantly under-predicted using the DNV (2017) 'undrained global' calculation. These results highlight disparities between the DNV design guidelines and the FE results and motivate the development of improved design expressions.

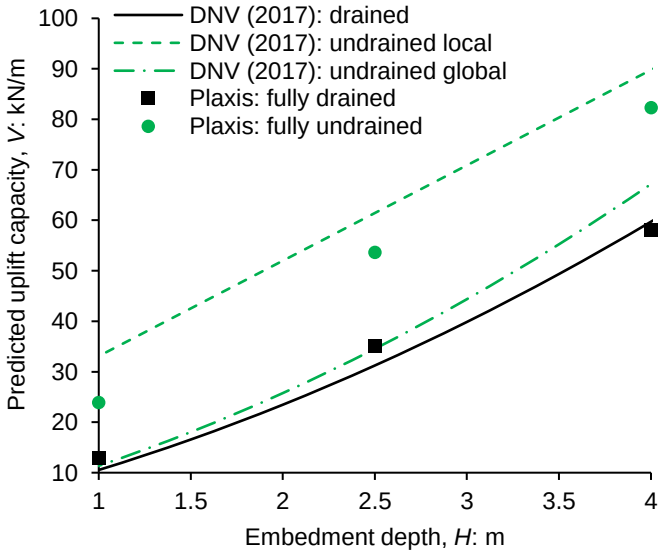

Fig. 5 Predictions of pipe uplift capacity for base case: comparison between present FE and DNV (2017); α = 0, soil profile 2, γ′ = 6 kN/m^3, ϕ′ = 30°, K = 0.5, N_c = 9

FINITE ELEMENT RESULTS

Base case results

Figure 6 presents exemplar FE predictions of the pipe load–displacement response for the base case scenario where the uplift velocities span six orders of magnitude. Also superimposed on the plot are markers indicating the peak resistance, V_{peak}, achieved over an uplift displacement of 0.1D. The plot shows that prior to any uplift displacement, a downward force is required to hold the pipe in position arising from a 'soil buoyancy' effect. It can be seen that for faster velocities, the load-displacement response is a smooth nonlinear curve. This contrasts with the near-bilinear load-displacement response observed for slower velocities. It is also noteworthy that no distinct peak in resistance is evident for the analyses with $\hat{v} < 0.3$.

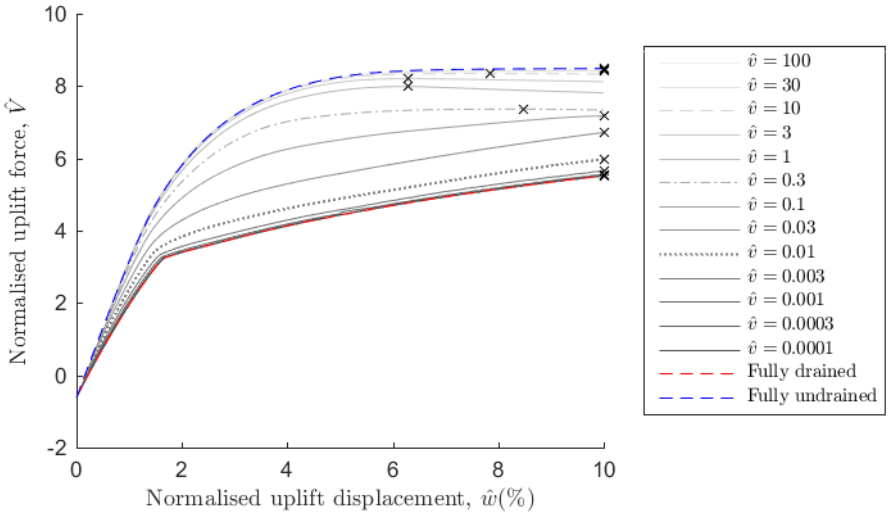

Fig. 6 Influence of pipe uplift rate on load–displacement response for base case; $\hat{H}$ = 2.5, soil profile 2, α = 0. The peak resistance achieved over an uplift displacement of 0.1D for each rate of uplift are indicated with '×'

The influence of pipe uplift velocity on the normalised peak resistance, $\hat{V}_{peak}$, is explored in Fig. 7. In these 'backbone' curves, the data points correspond to the peak uplift resistance achieved for a corresponding rate of uplift (see the markers in Fig. 6). The lines denoted 'fully drained' and 'fully undrained' represent the two extreme rates of uplift. These values were obtained by enforcing full dissipation and zero dissipation of excess pore pressures respectively during calculation stage three. The shaded region on the plot denotes the partially

drained region of response established for full flow penetrometers (Randolph and House, 2001). Figure 7 shows that there is a gradual transition from drained to undrained behaviour in the region $10^{-3} < \hat{v} < 30$. Henceforth, the terms 'undrained region' and 'drained region' are used to denote $\hat{v} > 30$ and $\hat{v} < 10^{-3}$ respectively. While there appears to be consensus between the FE results and the recommendations of Randolph and House (2001) for the undrained 'bound', there is a marked difference between the drained bounds due to the difference in the boundary conditions of this problem.

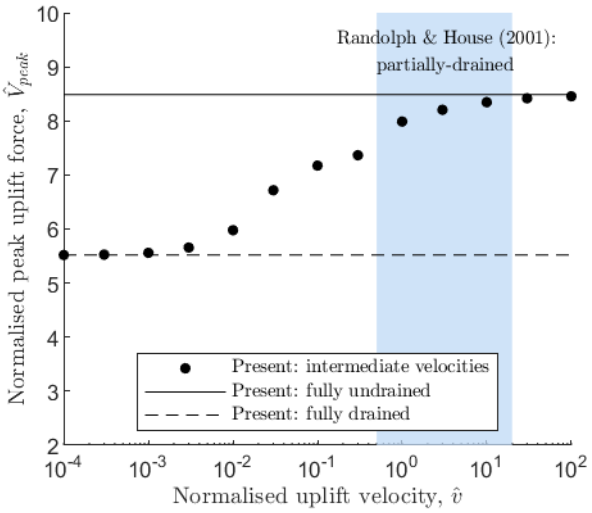

Fig. 7 Variation of normalised peak uplift resistance with normalised uplift rate for base case; $\hat{H}$ = 2.5, soil profile 2, α = 0. Shaded region denotes partially drained region of response applied to T-bar penetrometers (Randolph and House, 2001)

The effect of pipe uplift velocity on the soil failure mechanisms is shown in Fig. 8 using contours of incremental soil displacements. For $\hat{v}$ = 100 in Fig. 8(a), it can be seen that the failure mechanism corresponds to a local flow-around failure. A reduction in $\hat{v}$ causes the failure mechanism to transition to a sliding block with inclined slip surfaces. For slower uplift velocities, significant soil compression is evident directly above the pipe crown with less soil deformation beneath the pipe invert (due to reduced suction development).

(a)

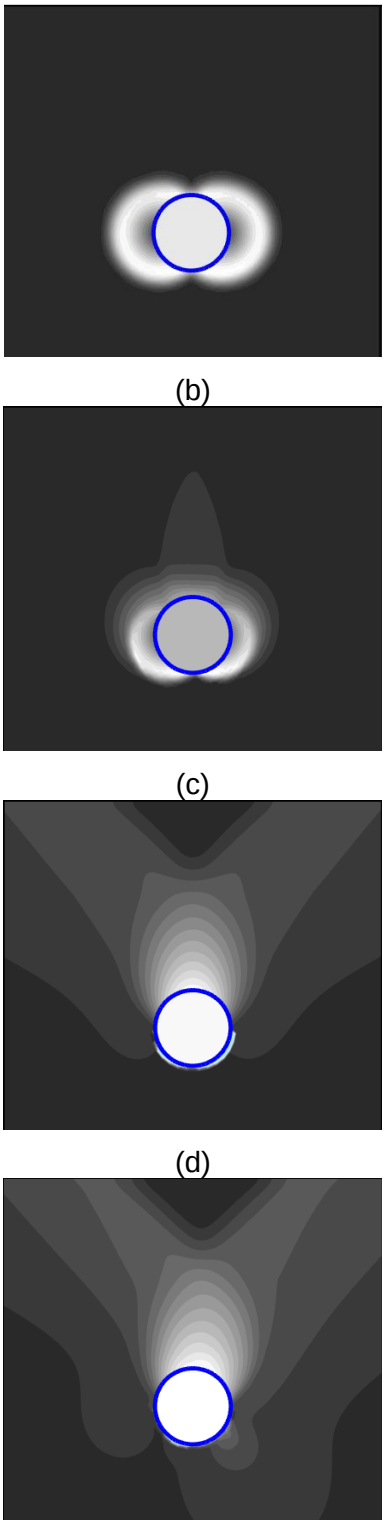

Fig. 8 Contours of incremental soil displacements showing soil failure mechanisms for values of $\hat{v}$ = (a) 10^{2}, (b) 10^{0}, (c) 10^{-2} and (d) 10^{-4}; base case, $\hat{H}$ = 2.5, profile 2, α = 0

Figures 9(a) – 9(c) show FE predictions of the development of excess pore pressures, Δu, during uplift determined at a single integration point located at the pipe crown, springline and invert respectively. From Fig. 9(a), it can be seen that undrained uplift generates compressive $\Delta \hat{u}$ above the pipe crown. It is also noteworthy that $\Delta \hat{u}$ generated at the pipe springline are considerably smaller than those generated at both the pipe crown and invert. It can also be seen that considerable suction develops at the pipe invert during fast uplift, as shown in Fig. 9(c).

(a)

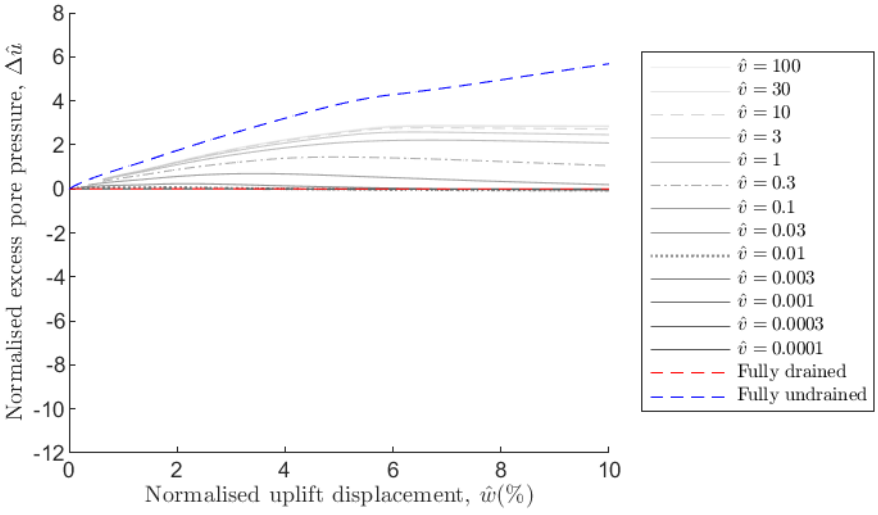

(b)

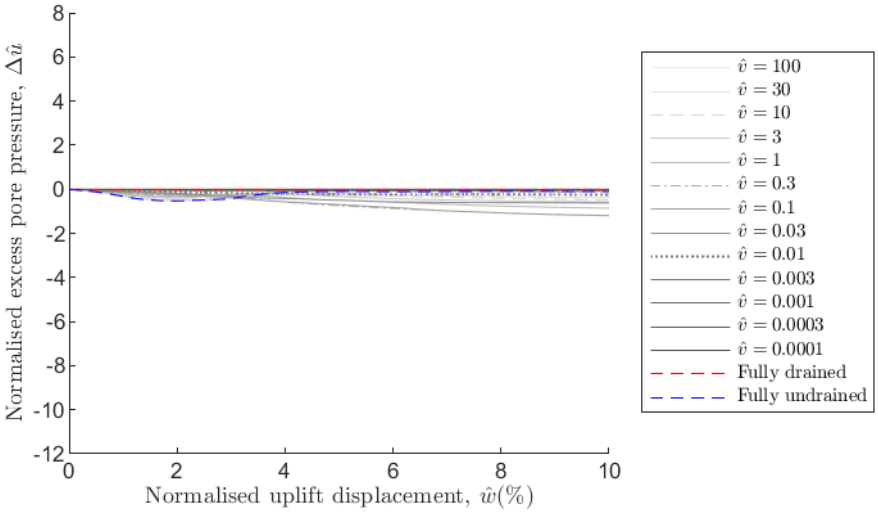

(c)

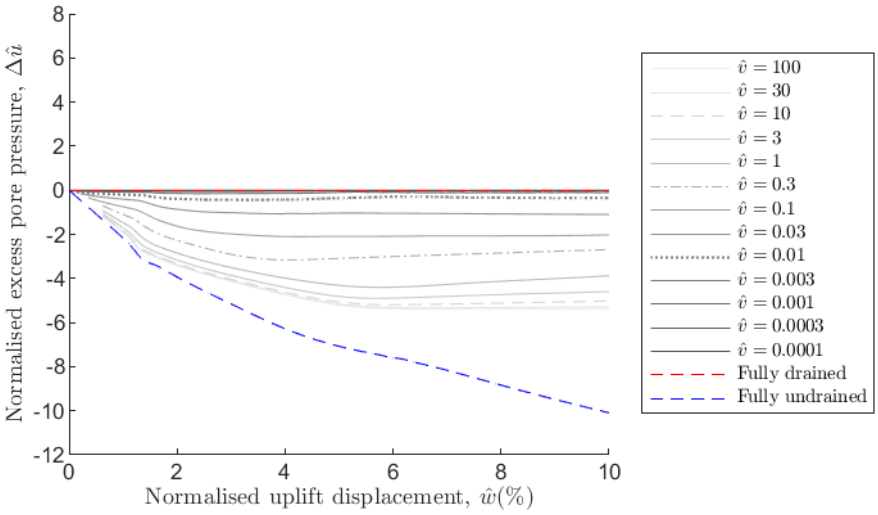

Fig. 9 Influence of pipe uplift displacement and uplift rate on the mobilisation of excess pore pressures (suction negative) determined from a single Gauss point located at the pipe (a) crown, (b) springline and (c) invert for base case analysis; $\hat{H}$ = 2.5, soil profile 2, α = 0.

In general, there appears to be some disparity between the results of $\Delta\hat{u}$ in Fig. 9 and $\hat{V}_{peak}$ in Fig. 7. Although predictions of $\hat{V}_{peak}$ determined for $\hat{v}$ = 100 and fully undrained conditions are almost identical, there exists notable differences between corresponding values of $\Delta\hat{u}$; this is evident at both the pipe crown and invert. Conversely, it can be seen that for $\hat{v}$ < 0.01, $\Delta\hat{u}$ is negligible (indicating a fully drained response) whereas the $\hat{V}_{peak}$ appears only partially drained. This suggests that pore pressures, as determined locally at the pipe-soil interface, may not be a robust indicator of whether the overall pipe uplift response is drained or undrained.

The development of normalised effective stress $\hat{\sigma}'$ (see Table 1) normal to the pipe-soil interface is explored in Fig. 10. Again, these results are determined from a single integration point located at the pipe crown (Fig. 10(a)), springline (Fig. 10(b)) and invert (Fig. 10(c)). Clearly slower uplift velocities allow greater dissipation of excess pore pressures generated during uplift. At the pipe crown, this causes an increase in compressive $\hat{\sigma}'_v$ during loading whereas at the pipe springline, $\hat{\sigma}'_h$ tends towards zero for $\hat{v} \leq 0.03$. At the pipe invert, the

development of $\hat{\sigma}'_v$ during uplift appears to be almost invariant to $\hat{v}$ and separation between pipe and soil ($\sigma'_v = 0$ at pipe invert) is mobilised at $\hat{w} \approx 1.5\%$.

(a)

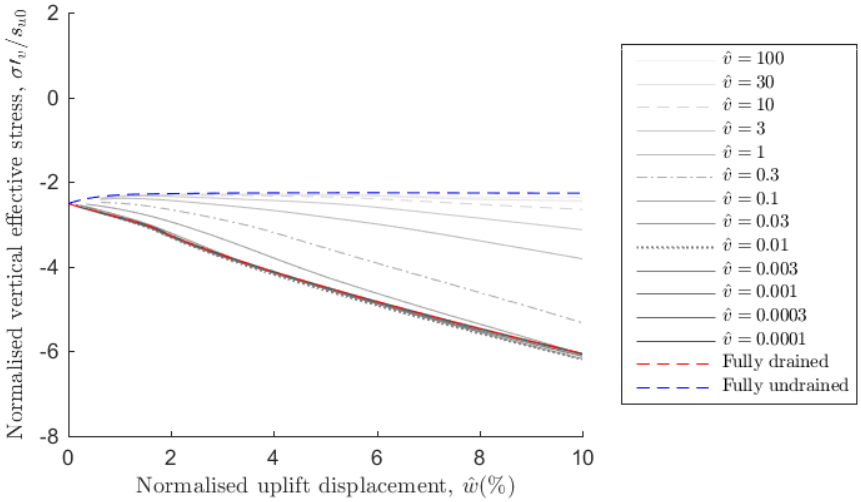

(b)

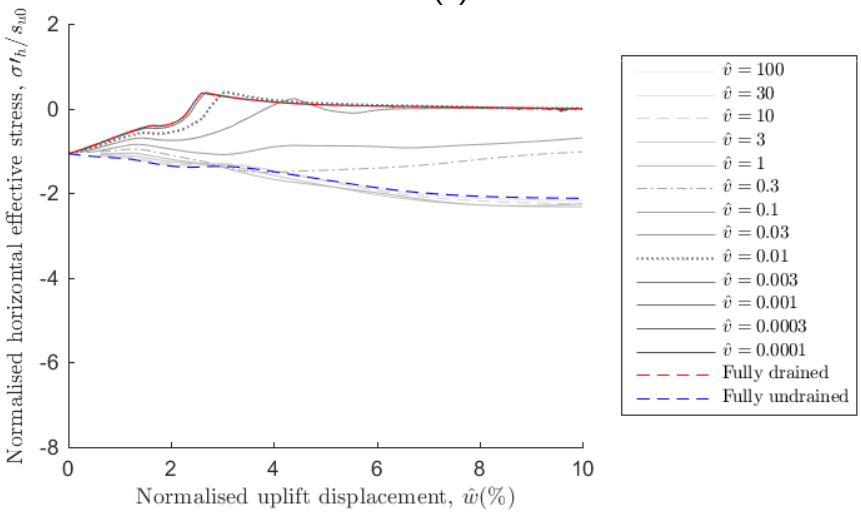

(c)

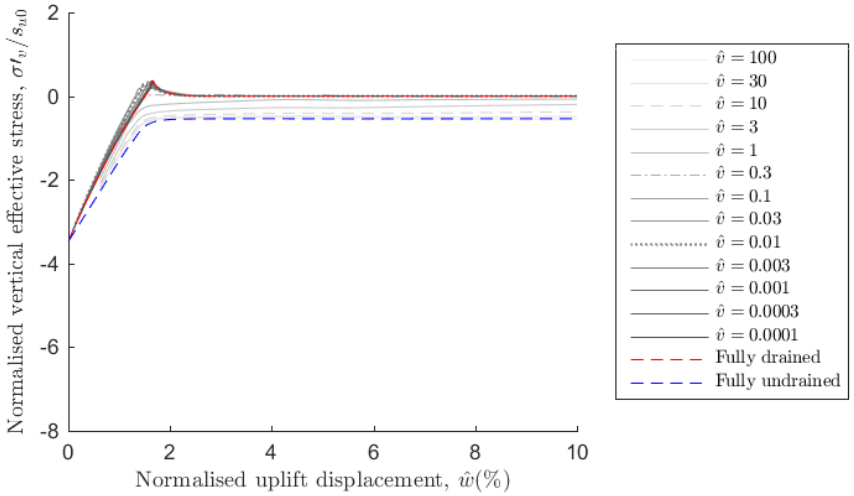

Fig. 10 Influence of pipe uplift displacement and uplift rate on the mobilisation of effective soil stresses (tension positive) determined from a single Gauss point located at the pipe (a) crown, (b) springline and (c) invert for base case analysis; $\hat{H}$ = 2.5, soil profile 2, α = 0.

Influence of pipe embedment depth

Figure 11 plots the backbone curves for the base case along with results determined for $\hat{H}$ = 1 and 4. Two different normalisations are considered for the uplift resistance in this and subsequent plots: $\hat{V}_{peak}$ (see Table 1; Fig. 11(a)), and V_{rel} (Fig. 11(b)) where V_{rel} is defined as the 'relative resistance' between drained and undrained as follows:

$$V_{rel} = \frac{V_{peak} - V_{peak,d}}{V_{peak,u} - V_{peak,d}} \quad (5)$$

where $V_{peak,d}$ and $V_{peak,u}$ are the FE-predicted fully drained and fully undrained peak uplift resistances respectively. As expected, an increase in $\hat{H}$ causes an upward shift in all values of $\hat{V}_{peak}$, as shown in Fig. 11(a). For a shallowly buried pipe, where the failure mechanism may propagate to the soil surface, it is plausible that the representative length dimension for drainage is H rather than D. Nevertheless, there is remarkable consistency between the three sets of results presented in Fig. 11(b), suggesting that the adopted normalisation for $\hat{v}$ is appropriate for the pipe / soil parameters considered here.

(a) (b)

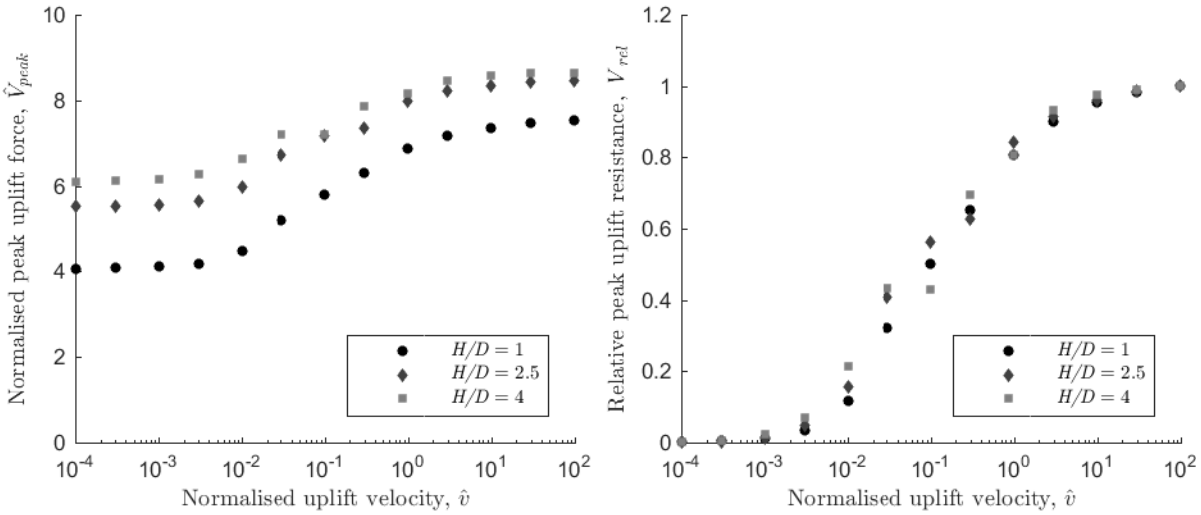

318

319 **Fig. 11** Influence of normalised embedment depth on the variation of peak resistance with
320 uplift rate for base case: (a) standard normalisation of uplift resistance ($\hat{V}_{peak}$), (b) alternative
321 normalisation of uplift resistance (V_{rel}); $\hat{H}$ = 2.5, soil profile 2, α = 0

322

323 *Influence of soil strength profile*

324 Figure 12 explores the role of the soil strength profile on the backbone curve. Four different
325 profiles are considered, the details of which are provided in Table 2. Figure 12(a) shows that,
326 in the undrained region, the largest values of $\hat{V}_{peak}$ correspond to soil profile 4 reflecting the
327 underlying more uniform soil strength with depth. However, the significant differences in $\hat{V}_{peak}$
328 in the drained region are somewhat misleading – this is largely attributable to the normalisation
329 by s_{u0} rather than differences in the *absolute* drained resistance. Using the alternative
330 normalisation in Fig. 12(b), it does appear that the soil profile has some influence on the shape
331 of the backbone curve, particularly at $\hat{v} \approx 0.1$.

332

333 *Influence of interface roughness*

334 Although the focus of this study is on the uplift resistance of smooth pipes, a limited number
335 of analyses considering a rough pipe have also been included here for comparison (see Fig.
336 13). It can be seen that although there are noteworthy, and indeed expected, differences in

the two sets of $\hat{V}_{peak}$ predictions in Fig. 13(a), the results presented in Fig. 13(b) are remarkably similar. The uplift velocities required to achieve drained and undrained resistance therefore appear to be insensitive to α.

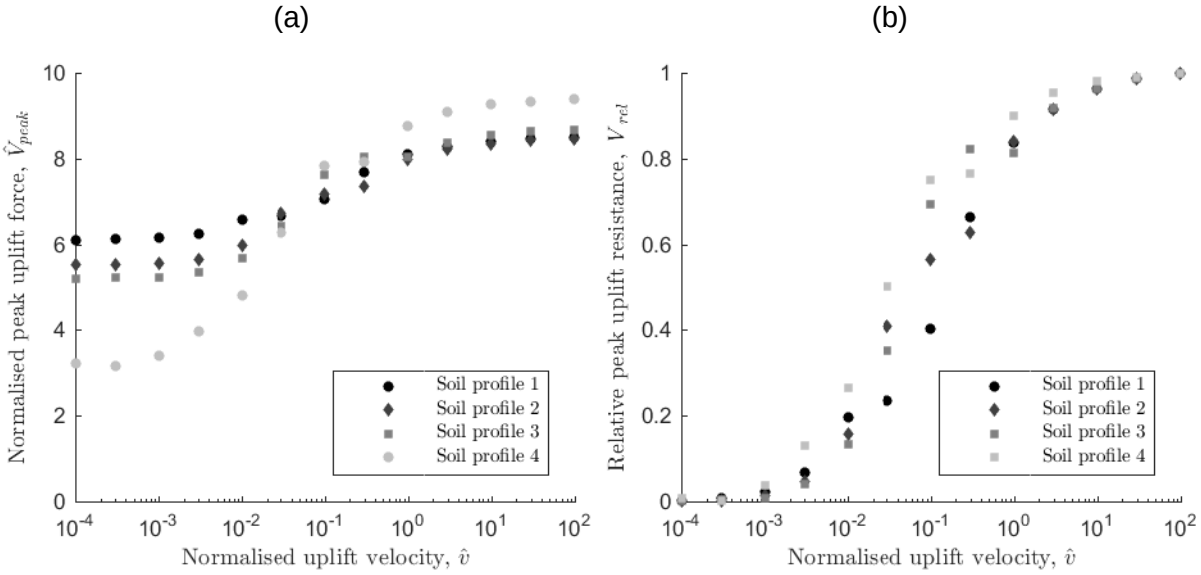

Fig. 12 Influence of soil strength profile on the variation of peak uplift force with uplift rate: (a) standard normalisation of uplift resistance ($\hat{V}_{peak}$), (b) alternative normalisation of uplift resistance (V_{rel}); $\hat{H}$ = 2.5, α = 0

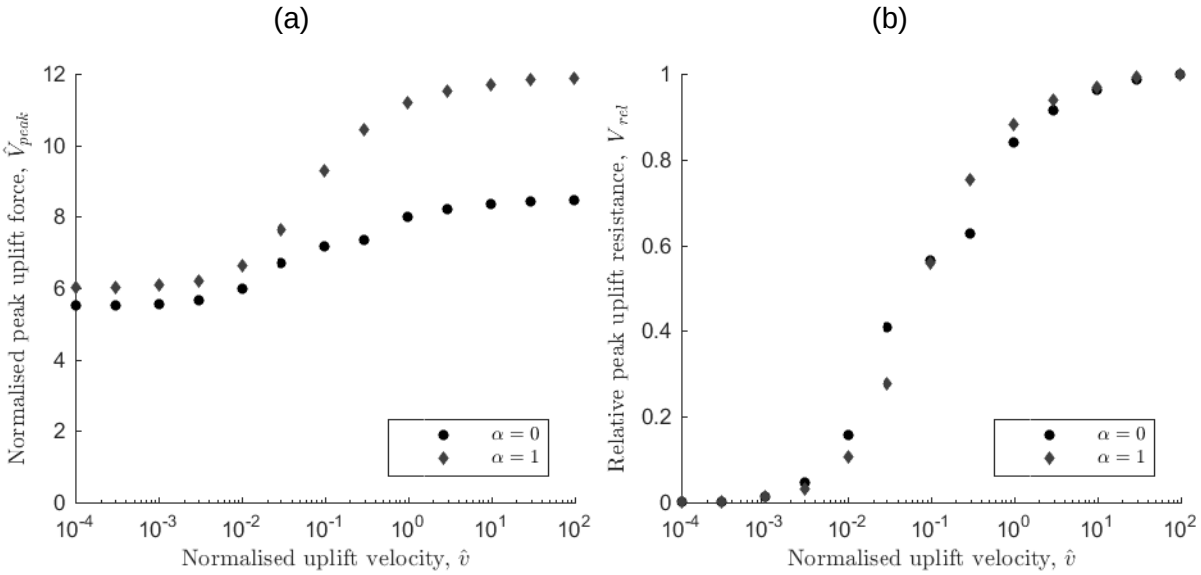

Fig. 13 Influence of interface roughness on the variation of peak uplift force with uplift rate: (a) standard normalisation of uplift resistance ($\hat{V}_{peak}$), (b) alternative normalisation of uplift resistance (V_{rel}); $\hat{H}$ = 2.5, α = 0

DESIGN CALCULATION ACCOUNTING FOR UPLIFT VELOCITY

Design method development

Oliveira et al. (2011) developed an expression for predicting the partially drained shear resistance of clay, applied to the T-bar penetrometer test:

$$s_p = s_u \left(1 + \frac{b - 1}{1 + \left(\frac{\hat{v}}{n} \right)^{\frac{4c}{b-1}}} \right) \quad (6)$$

where s_p is any intermediate partially drained shear strength between drained and undrained conditions, s_u is the undrained shear strength, the parameter b defines the ratio between the drained strength and undrained strength, the parameter n defines the midpoint of the transition curve, and parameter c controls the shape of the curve.

For the present work, this expression was modified as:

$$V = V_{peak,d} + \frac{V_{peak,u} - V_{peak,d}}{1 + \left(\frac{n}{\hat{v}} \right)^{\frac{4c}{b-1}}} \quad (7)$$

where V is any intermediate partially drained uplift capacity and, in this instance, the parameter $b = V_{peak,u}/V_{peak,d}$. For the purpose of calibrating equation (7), the variables $V_{peak,u}$, $V_{peak,d}$ and hence b were determined directly from the FE output. Parameters n and c were obtained by curve fitting equation (7) to the FE results using a nonlinear generalized reduced gradient algorithm and least squares goodness of fit. Results from all 180 combinations of parameters listed in Tables 2 and 3 and for $\hat{H}$ = 1, 2.5, 4 were used in the curve-fitting process. Conveniently, strong linearity between the two curve-fitting parameters (c and n) and the

parameter b was observed. A linear least squares regression provides the following expressions for c and n:

$$c = 0.197b - 0.208 \quad (8)$$

$$n = -0.015b + 0.119 \quad (9)$$

Interestingly, the curve-fitting parameters are independent of the soil profile and the pipe embedment depth. The proposed calculation methodology can therefore be defined as follows:

I. The fully undrained uplift capacity, $V_{peak,u}$, is determined using numerical analysis or solutions previously documented in the literature e.g. Martin and White (2012).
II. The drained uplift capacity is determined using the calculation given in DNV (2017; see equation (1)). This calculation shows good agreement with the FE predictions provided an appropriate value of K is adopted (see Fig. 5).
III. The parameter b is determined as $V_{peak,u}/V_{peak,d}$.
IV. The parameters c and n are determined as functions of b using equations (8) and (9).
V. The partially drained uplift capacity, V, is determined from the normalised uplift velocity $\hat{v}$ using equation (7).

The design methodology outlined in steps I to V above is verified by re-predicting the FE results. Figure 14 shows an exemplar fit to the FE prediction of the base case (refer to Table 3 for parameters). Furthermore, predictions of pipe uplift capacity determined using equation (7) are compared to the FE output for all 180 analyses in Fig. 15. In both instances, equation (7) appears to provide a high fidelity representation of the FE data.

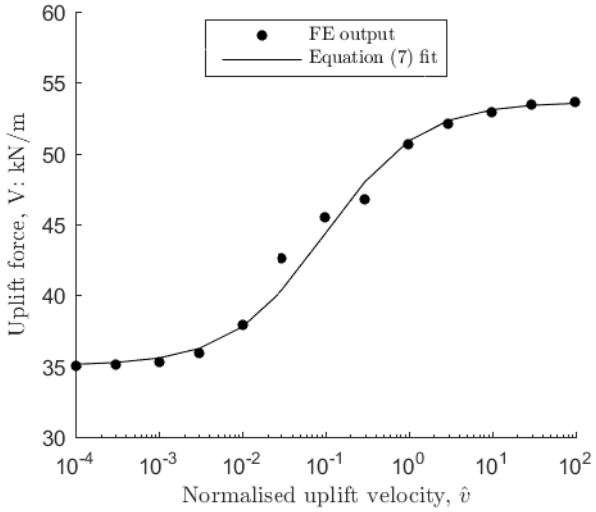

387

388 **Fig. 14** Exemplar fit between equation (7) and FE output for base case; $\hat{H}$ = 2.5, soil profile
389 2, α = 0. Parameters *c* and *n* determined using equations (8) and (9) respectively

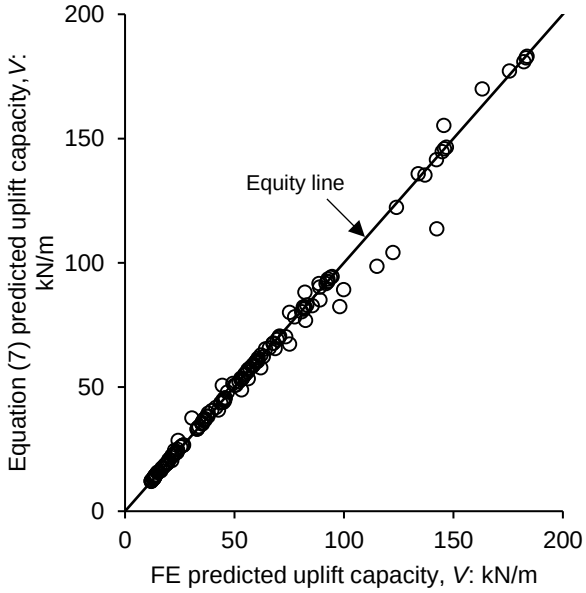

390

391 **Fig. 15** Verification of uplift capacity predictions determined using proposed design method
392 through comparisons to FE predictions; all analyses with α = 0

393

394 *Application: hypothetical design scenario*

395 The proposed design methodology is applied to a hypothetical design scenario using typical
396 parameters encountered in practice (listed in Table 4). It is assumed that the undrained shear
397 strength profile can be described as $s_u = s_{um} + \rho z$ where s_{um} is the shear strength at mudline
398 level and ρ is the gradient of strength with depth. The parameter $V_{peak,u}$ for each embedment

399 depth is determined using OxLim assuming full-tension interface conditions whereas $V_{peak,d}$ is
400 determined using the DNV (2017) drained calculation. Uplift capacity predictions for a 0.4 m
401 diameter pipe and for embedment depths covering 0.4 m to 1.6 m ($\hat{H}$ between 1 and 4) are
402 plotted in Fig. 16. In this instance, it can be seen that the uplift velocity required to achieve
403 fully drained and fully undrained capacity is approximately 0.001 m/year, or 0.0025*D* per year,
404 and 10 m/year, or 25*D* per year, respectively. Given that the drained calculation is typically
405 the limiting design case for pipelines buried offshore, the former rate of loading is very low and
406 may not be realistic from a design viewpoint.

407

408 **Table 4** Pipe / soil parameters adopted for example design case

Parameter	Value
Pipe diameter, D (m)	0.4
Effective soil unit weight, γ' (kN/m^3)	6.5
Undrained shear strength at mudline, s_{um} (kpa)	5
Increment of strength with depth, ρ (kPa / m)	1.0
Soil friction angle, ϕ' (°)	30
Coefficient of lateral earth pressure, K	0.5
Coefficient of consolidation, c_v (m^2/year)	1

409

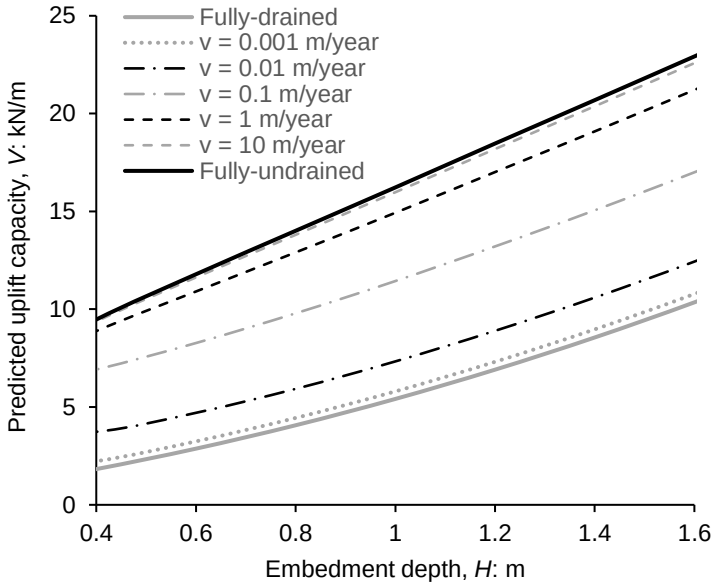

410

411 **Fig. 16** Predictions of pipe uplift capacity as a function of embedment depth for various rates
412 of uplift for hypothetical design scenario (see Table 4 for parameters)

413

414 *Limitations of method*

415 In reality, for the pipe uplift problem there is likely to be a significant post-peak reduction in
416 capacity arising from the changing geometry (continuous reduction of embedment), possibly
417 accompanied by non-ductile material response. In particular, for shallowly buried pipes the
418 peak capacity may be accompanied by rupture planes propagating to the soil surface, so that
419 the post-peak capacity rapidly degrades perhaps to just the weight of soil in the wedge above
420 the pipe. Rationally incorporating crack development in the overlying soil within a numerical
421 model is highly complex. The present study is focused on the initial part of the pipe uplift
422 process where there is no loss of integrity of the backfill soil. In this study, the soil backfill was
423 also assumed to be locally homogeneous. The value of c_v to be used in equation (7) should
424 be representative of the backfill material encountered in practice comprising a matrix of blocks
425 and slurry-filled voids (Yang et al. 2002).

426 The undrained shear strength parameter s_{u0} used in the uplift resistance calculation should
427 also be representative of the applied loading rate. It may be appropriate to modify strengths

inferred from cone penetration test results, or full flow penetrometer tests, to account for the slower rates of loading likely in a pipe uplift design scenario.

The adopted ‘wished-in-place’ pipe installation approach neglects potential ‘rigid inclusion’ effects arising from the soil backfilling process. This is on account of the pipe effectively behaving as a rigid body within the compressible soil backfill, thereby attracting a greater proportion of the overburden pressure. Rigorous treatment of the effect of the trenching method on the eventual undrained strength profile and coefficient of lateral earth pressure is required, to ensure appropriate values are used during the design process. The design method described in this paper assumes that an adequate assessment of this process has been completed.

CONCLUSIONS

This paper has described a finite element study of the behaviour of a plane strain pipe segment embedded in modified Cam clay soil subjected to various rates of uplift. Coupled-consolidation analyses were used to explore the role of rate effects on pipe uplift capacity and the transition between drained and undrained behaviour. Additional parameters considered in the modelling include pipe embedment depth, soil strength profile, and pipe-soil interface roughness. The guidance provided by the DNV (2017) design codes was appraised through comparisons to the FE results. This exercise revealed good agreement between drained capacity predictions if an appropriate coefficient of lateral earth pressure is adopted. Conversely, undrained predictions showed considerable divergence.

The numerical results also showed that the partially drained region of response, as determined from the peak uplift resistances, for the pipe uplift problem spans over four orders of magnitude, considerably greater than bounds previously established for full-flow penetrometers. The partially drained region of response also appears to be independent of the pipe / soil parameters considered here. The results also suggests that excess pore

pressures determined locally at the pipe-soil interface may not be a reliable means of determining whether the overall response is ‘drained’ or ‘undrained’.

A new closed-form design approach was developed and calibrated directly from the FE output. The predictive approach allows the uplift capacity to be determined as a function of the uplift velocity rather than assuming one of two extreme rates of uplift i.e. drained or undrained. The drained calculation is typically the limiting design case for pipelines buried offshore. However, application of the proposed design approach to a hypothetical design scenario revealed that the loading rate required to achieve this resistance is very low and may not be realistic from a design viewpoint.

In this study, simplifying assumptions have necessarily been adopted to numerically model the pipe uplift problem. Nevertheless, the present results suggest interesting pipe uplift behaviours. Further experimental validation of the presented results and the developed design methodology is clearly desirable to inform future developments considering, for example, spatial variations in soil properties to account for the pipe installation process, tension crack development in the overlying soil and three-dimensional pore water flow.

NOTATION LIST

A_p Cross-sectional area of the pipe.

b Curve-fitting parameter defining the ratio between drained strength and undrained strength.

c Curve-fitting parameter controlling the share of the strength curve.

c_v Coefficient of consolidation of soil.

D Pipe diameter.

e_0 Initial void ratio used for the determination of c_v.

H Soil cover height measured from the pipe crown.

$\hat{H}$ Normalised pipe embedment depth (see Table 1).

k Soil permeability

K ‘Operational’ coefficient of lateral earth pressure used in DNV (2017) design method.

K_0 In-situ ‘at-rest’ coefficient of lateral earth pressure for soil backfill.

M Slope of critical state line for modified Cam clay model.

n Curve-fitting parameter defining the midpoint of the strength transition curve.

N_c Undrained bearing capacity factor.

s_p Any intermediate partially drained shear strength between drained and undrained conditions.

s_u Undrained shear strength of the soil.

$\bar{s_u}$ Average undrained shear strength along failure planes extending from the centre of the pipe to the soil surface.

s_{um} Undrained shear strength at mudline level.

s_{u0} Initial undrained shear strength of the soil at the level of the pipe springline.

t Time.

v Pipe uplift velocity.

$\hat{v}$ Normalised pipe uplift velocity (see Table 1).

V Pipe uplift resistance.

V_{peak} Peak uplift resistance achieved over an uplift displacement of 0.1D.

$V_{peak,d}$ Fully drained peak uplift resistance achieved over an uplift displacement of 0.1D.

$V_{peak,u}$ Fully undrained peak uplift resistance achieved over an uplift displacement of 0.1D.

V_{rel} Relative pipe uplift resistance between drained and undrained values.

$\hat{V}$ Normalised pipe uplift resistance (see Table 1).

w Pipe uplift displacement.

$\hat{w}$ Normalised pipe uplift displacement (see Table 1).

z Depth below mudline level.

α Soil-structure interface roughness.

γ′ Effective unit weight of the soil backfill.

γ_w Unit weight of water.

Δu Excess pore water pressure.

$\Delta\hat{u}$ Normalised excess pore water pressure (see Table 1).

κ Slope of unloading-reloading line for modified Cam clay model.

λ Slope of normal compression line for modified Cam clay model.

ν'_{ur} Effective Poisson's ratio for modified Cam clay model.

ρ Increment of undrained shear strength with depth.

$\hat{\sigma}'$ Normalised effective soil stress (see Table 1).

σ'_h Horizontal effective soil stress.

σ'_v Vertical effective soil stress.

ϕ′ Friction angle of the soil backfill.

REFERENCES

Bransby, M. F., Newson, T. A., Brunning, P., 2002. Centrifuge modelling of the upheaval capacity of pipelines in liquefied clay. In *The Twelfth International Offshore and Polar Engineering Conference*. International Society of Offshore and Polar Engineers.

Cheuk, C.Y., Take, W.A., Bolton, M.D., Oliveira, J.R.M.S., 2007. Soil restraint on buckling oil and gas pipelines buried in lumpy clay fill. *Engineering structures*, 29, 6, 973-982.

DNV 2017. DNVGL-RP-F114. Pipe-soil interaction for submarine pipelines. Det Norske Veritas (DNV), Oslo, Norway.

Eiksund, G., Langø, H., Øiseth, E., 2013. Full-scale test of uplift resistance of trenched pipes. *International Journal of Offshore and Polar Engineering*, 23, 4, 298-306.

Koochekali, A., Gatmiri, B., Koochekali, A. A., 2013. Pipeline upheaval buckling in clayey backfill using numerical analysis. *International Journal of Marine Science and Engineering*, 3, 2, 43-50.

Makrodimopoulos, A., Martin, C.M. 2006. Lower bound limit analysis of cohesive-frictional materials using second-order cone programming. *International Journal for Numerical Methods in Engineering*, 66, 4, 604-634.

536 Makrodimopoulos, A., Martin, C.M. 2007. Upper bound limit analysis using simplex strain
537 elements and second-order cone programming. *International Journal for Numerical and*
538 *Analytical Methods in Geomechanics*, 31, 6, 835-865.
539 Makrodimopoulos, A. & Martin, C.M. 2008. Upper bound limit analysis using discontinuous
540 quadratic displacement fields. *Communications in Numerical Methods in Engineering*, 24,
541 11, 911-927.
542 Martin, C.M. 2011. The use of adaptive finite-element limit analysis to reveal slip-line fields.
543 *Géotechnique Letters*, 1, 2, 23-29.
544 Martin, C. M., White, D. J., 2012. Limit analysis of the undrained bearing capacity of offshore
545 pipelines. *Géotechnique*, 62, 9, 847-863.
546 Newson, T. A., Deljoui, P., 2006. Finite element modelling of upheaval buckling of buried
547 offshore pipelines in clayey soils. In *Soil and Rock Behavior and Modeling*, 351-358.
548 Oliveira, J. R. M. S., Almeida, M.S.S., Motta, H.P.G., Almeida, M.C.F. 2011. Influence of
549 penetration rate on penetrometer resistance. *Proc ASCE Journal of Geotechnical and*
550 *Geoenvironmental Engineering,* 137, 7, 695-703.
551 Randolph, M. F., Houlsby, G. T. 1984. The limiting pressure on a circular pile loaded laterally
552 in cohesive soil. *Géotechnique,* 34, 613-623.
553 Randolph, M. F., House, A. R. 2001. The complementary roles of physical and computational
554 modelling. *Int. J. of Physical Modelling in Geotechnics,* 1, 1, 1–8.
555 Schaminee, P. E. L., Zorn, N. F., Schotman, G. J. M. 1990. Soil response for pipeline upheaval
556 buckling analyses: full-scale laboratory tests and modelling. *Proceedings of the 22nd*
557 *Annual Offshore Technology Conference.* Houston, TX, USA.
558 Thusyanthan, N. I., Ganesan, S. A., Bolton, M. D., Allan, P., 2008. Upheaval buckling
559 resistance of pipelines buried in clayey backfill. In *The Eighteenth International Offshore*
560 *and Polar Engineering Conference*. International Society of Offshore and Polar Engineers.
561 Trautmann, C. H., O'Rourke, T. D., Kulhaway, F. H. 1985. Uplift force-displacement response
562 of buried pipe. *Journal of Geotechnical Engineering,* 11**,** 1061-1076.
563 Wang, J., Haigh, S. K. and Thusyanthan, N. I., 2009. Uplift resistance of buried pipelines in
564 blocky clay backfill. In *Proc. International Offshore (Ocean) and Polar Engineering*
565 *Conference*.
566 Wood, D.M., 1990. *Soil behaviour and critical state soil mechanics*. Cambridge university
567 press.
568 Yang, L. A., Tan, T. S., Tan, S. A., Leung, C. F. 2002. One-dimensional self-weight
569 consolidation of a lumpy clay fill. *Géotechnique* 52, 716-725.